Proceedings of the 3rd IASME/WSEAS Int. Conf. on FLUID DYNAMICS & AERODYNAMICS, Corfu, Greece, August 20-22, 2005 (pp261-266)

Fully Conservative Discretizations for Local Grid Refinement

A.J.A. KORT, R.W.C.P. VERSTAPPEN, F.W. WUBS AND A.E.P. VELDMAN
Department of Mathematics
University of Groningen
P.O. Box 800, 9700 AV Groningen
THE NETHERLANDS
kort@math.rug.nl http://www.math.rug.nl/~veldman

Abstract: - For performing simulations of turbulent channel flow, it is of great importance that the balance between convective transport and dissipation remains undisturbed. We ensure this by using a symmetry-preserving discretization of the Navier-Stokes equations. In such a discretization, crucial properties of differential operators are mimicked by the corresponding difference operators. This makes a symmetry-preserving discretization stable on any grid and lets it conserve mass, momentum and, in absence of diffusion, kinetic energy. Because we want to reduce the computational effort as well, we make a symmetry-preserving discretization capable of dealing with local grid refinement. The discretization was tested for Poiseuille flow at relatively low Reynolds numbers. The results encourage us to use the method for a turbulent flow around a square cylinder at $Re = 22000$ in the future.

Key-Words: - Conservative discretization, local grid refinement, direct numerical simulation, turbulence

1 Symmetry-preservation

Fluid motion is well described by the Navier-Stokes equations, which constitute conservation laws for mass and momentum. We discretize them with a finite-volume discretization. The discretization is performed in such a way that the difference operators do have the same symmetry properties as the underlying differential operators, This means that the convective operator is represented by a skew-symmetric coefficient matrix C, so

$$C + C^* = 0, \tag{1}$$

and the diffusive operator by a symmetric, negative-definite matrix D. Also, the discrete gradient matrix G, describing the integration of the (pressure) gradient operator over the control volumes V, is related to the discrete divergence matrix M, describing the integration of the divergence (of the velocity) over the control volumes V, as

$$G = -M^*. \tag{2}$$

This corresponds to the fundamental, analytical relation

$$\nabla = -(\nabla\cdot)^*. \tag{3}$$

Such a symmetry-preserving discretization does not only conserve mass and momentum, but also energy (in absence of diffusion of course). Because, if we write the Navier-Stokes equations in semi-discretized form as

$$M\mathbf{u}_h = \mathbf{0} \tag{4}$$

$$\frac{\mathrm{d}}{\mathrm{d}t}V\mathbf{u}_h = C\mathbf{u}_h + D\mathbf{u}_h + M^*\mathbf{p}_h \tag{5}$$

with $\mathbf{u}_h$ the discrete velocity and $\mathbf{p}_h$ the discrete pressure, the energy $\langle V\mathbf{u}_h, \mathbf{u}_h\rangle$ evolves as

$$\begin{aligned}\frac{\mathrm{d}}{\mathrm{d}t}\langle V\mathbf{u}_h, \mathbf{u}_h\rangle &= \langle\frac{\mathrm{d}}{\mathrm{d}t}V\mathbf{u}_h, \mathbf{u}_h\rangle + \langle V\mathbf{u}_h, \frac{\mathrm{d}}{\mathrm{d}t}\mathbf{u}_h\rangle \\ &= \langle\frac{\mathrm{d}}{\mathrm{d}t}V\mathbf{u}_h, \mathbf{u}_h\rangle + \langle\mathbf{u}_h, \frac{\mathrm{d}}{\mathrm{d}t}V\mathbf{u}_h\rangle \\ &\overset{(1),(2)}{=} \langle(D + D^*)\mathbf{u}_h, \mathbf{u}_h\rangle \\ &\leq 0. \end{aligned} \tag{6}$$

This also shows, just as it should be, the absence of interference between the convection and the diffusion. With that, we have reached our main reason for studying this kind of discretizations. Because we want to simulate turbulent flows, we want to avoid artificial dissipation interfering with the subtle balance between convective transport and physical dissipation. Furthermore, (6) also shows the stability of the discretization on any grid.

One should realize that a symmetry-preserving discretization does not minimize the local truncation error; it performs well because of the favourable properties of the discrete operators (see also [6] and [7]).

2 Local grid refinement

We make the conservative discretizations suitable for local grid refinement because of the reduction of com-

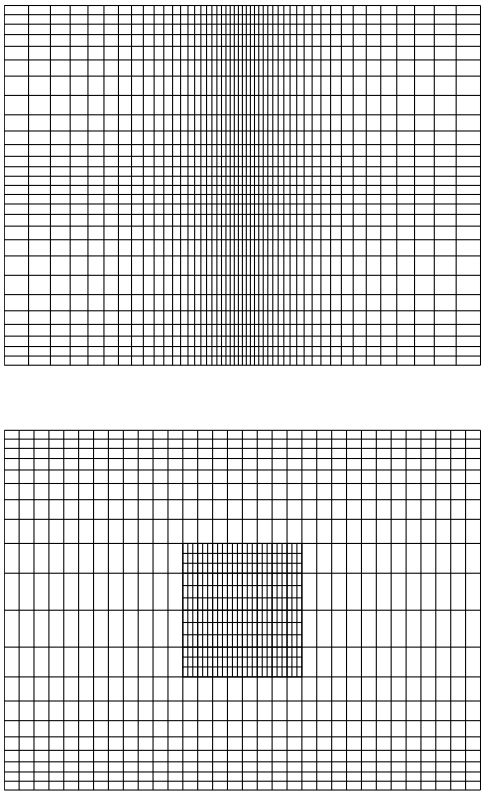

Figure 1: The reduction of cells achieved by local grid refinement. The stretched grid has 1344 cells. The locally refined grid counts only 896 cells.

putational effort that can be achieved by local grid refinement. An example of this reduction is given in Figure 1. As one can see, local grid refinement saves on the amount of computational cells needed and thus it saves on the amount of computational time needed to perform a simulation.

In this paper, we will discuss the 2D-case. A 3D-discretization can be obtained from the 2D-case straightforward as long as no refinement is created in the third direction.

We start with a uniform grid. Stretching can be applied to refine along the boundaries of the computational domain. Thereafter, the local refinement is obtained by uniformly splitting the cells within a designated rectangular area in the computational domain into nine. So 3:1-refinement is created. Figures 1 and 2 show such situations. We choose 3:1-refinement because then there is a velocity defined at all coarse grid points. Perhaps we can benefit from this natural refinement in the construction of our discretizations. Depending on the resolution needed, the refinement procedure can be repeated. The levels of refinement are successively numbered starting with 0, which de-

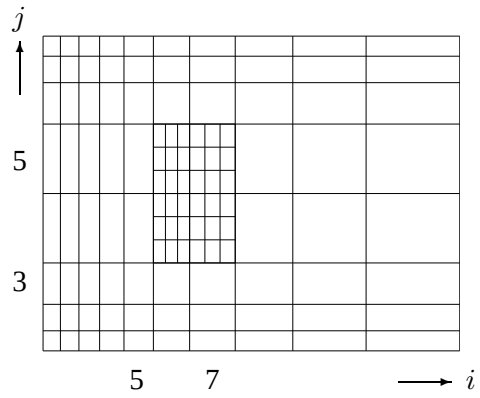

Figure 2: An example of a grid with local refinement. The shown row and column numbers are used for marking the position of the refined area.

notes the coarsest level. At every level, the cells are numbered using an (i, j)-index notation. So, every cell has three indices. An indicator "function" is used for determining whether a cell or velocity is at the current level.

By referring to the coarse row and column indices at the refinement boundary all neighbours can be found by simple calculations. We denote the minimum and maximum refinement boundary indices in the i-direction with $minib$ and $maxib$. Similarly, we have $minjb$ and $maxjb$ in the j-direction. In Figure 2, these boundary indices are $minib = 5$, $maxib = 7$, $minjb = 3$ and $maxjb = 5$. Then, for example, the middle northern neighbour of cell $(ci, minjb; 0) = (6, 3; 0)$ is $(\mathit{fi}, 1; 1)$ with fi given by

$$\begin{aligned} \mathit{fi} &= (ci - minib - 1) * 3 + 2 \\ &= (6 - 5 - 1) * 3 + 2 \\ &= 2. \end{aligned} \tag{7}$$

In more general situations, a quadtree numbering can be used (e.g. see [1] and [5]).

3 Performing the discretization

Away from refinement boundaries, conservative discretizations can easily be constructed. At refinement boundaries, we have to do some more work, because here the discretization becomes irregular. But in both cases the same way of reasoning is used. First the sum of momentum fluxes is determined over the boundary of the conservation cell of a velocity component. For example, we determine the discrete version of $\int_S u\mathbf{u}^T \cdot \mathbf{n}\, dS$, which is the convective term in the x-direction ($\mathbf{u}^T = (u, v)^T$ denotes the velocity with u and v the velocity components in the x- and y-direction respectively, S is the boundary of the con-

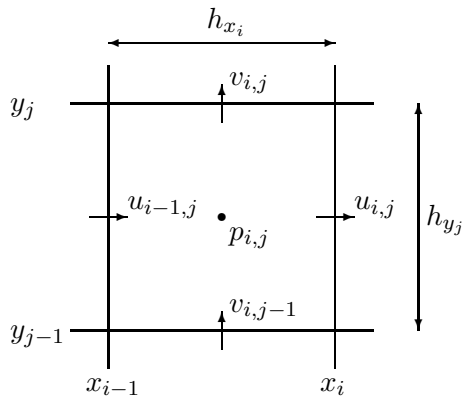

Figure 3: The variables of cell (i, j).

servation cell and **n** represents the outward pointing normal). In this term, u is the unknown and its coefficient $\mathbf{u}^T \cdot \mathbf{n}$ will lead to (a part of) the convective matrix. Thereafter, the mass fluxes in this sum are chosen such that the central coefficient becomes zero, for only then a skew-symmetric convective matrix will be obtained. The discrete divergence (4) plays an important role in this last process.

That brings us to another problem that we should consider: what is the divergence in the cells along a refinement boundary? Because of relation (2), an equivalent question is: what is the pressure gradient over the refinement boundary?

We want the discrete divergence to obey

$$M\mathbf{u}_{h;const} = \mathbf{0} \tag{8}$$

and the discrete gradient to obey

$$V^{-1}G\mathbf{p}_{h;lin} = \mathbf{c} \tag{9}$$

in which $\mathbf{u}_{h;const}$ denotes a velocity field $u_{i,j} = c$ with c a constant and $v_{i,j} = 0$, $\mathbf{p}_{h;lin}$ represents a linear pressure field $p_{i,j} = c_1 x_i + c_2 y_j + c_3$ (with c_1,c_2 and c_3 constants) and **c** is the appropriate constant vector describing the inclination of the pressure plane. For if equations (8) and (9) are not fulfilled, then our discretization is not even first order.

We start with defining the gradient matrix. Then the divergence follows by (2). To construct the gradient matrix, we have to define the "missing" pressures. With respect to Figure 4 (see Figure 3 for the general positioning of the variables), $p_{2,4;1}$ and $p_{2,6;1}$ are missing an eastern neighbour for example. We can not use linear interpolation to set up the gradient matrix, because it gives a divergence that is in conflict

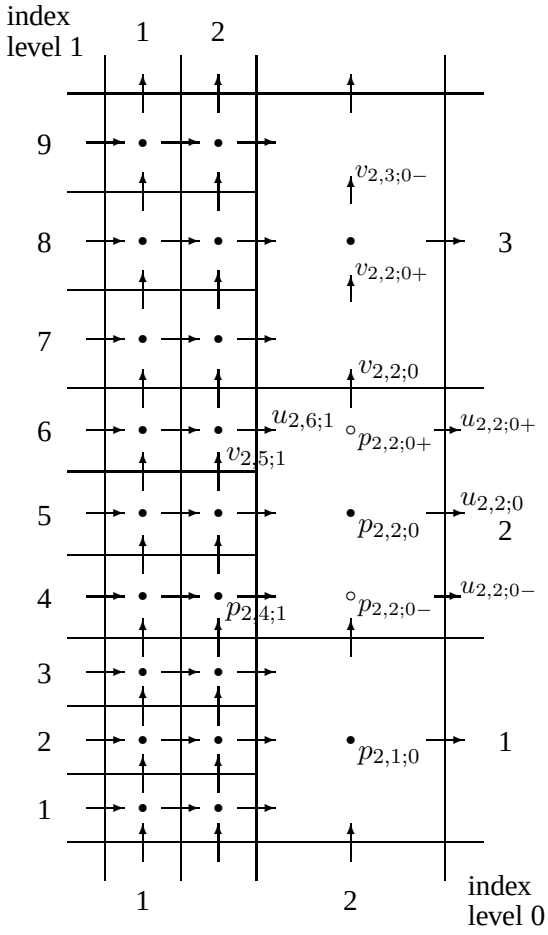

Figure 4: A piece of a refinement boundary. The index numbering has been adapted to the size of the piece. Compare Figure 3 for the placement of the variables. Ghost variables are shown in small print.

with equation (8). The problem can be solved by using a larger stencil for the approximations of the ghost pressures. We do this by using

$$p_{2,2;0-} = p_{2,2;0} - \frac{h_{y_{5;1}}(p_{2,3;0} - p_{2,1;0})}{\frac{1}{2}h_{y_{3;0}} + h_{y_{2;0}} + \frac{1}{2}h_{y_{1;0}}}, \tag{10}$$

$$p_{2,2;0+} = p_{2,2;0} + \frac{h_{y_{5;1}}(p_{2,3;0} - p_{2,1;0})}{\frac{1}{2}h_{y_{3;0}} + h_{y_{2;0}} + \frac{1}{2}h_{y_{1;0}}}. \tag{11}$$

We explain these extrapolations with help of Figure 5. At first, we know the y-positions and values of $p_{2,1;0}$, $p_{2,2;0}$, $p_{2,3;0}$. Further, we know the y-positions of the missing pressures $p_{2,2;0-}$ and $p_{2,2;0+}$. The curve in the figure represents the solution which we want to approximate. In the first step, the slope of the line between $p_{2,1;0}$ and $p_{2,3;0}$ is determined. This slope is

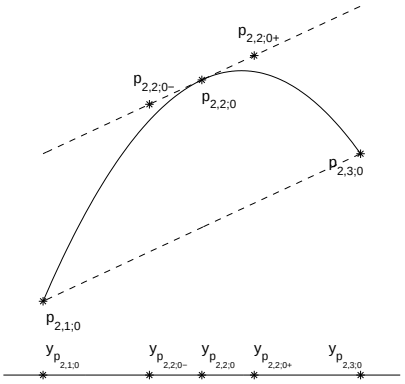

Figure 5: The construction of the approximation of the missing pressures.

$\frac{p_{2,3;0}-p_{2,1;0}}{y_{p_{2,3;0}}-y_{p_{2,1;0}}} = \frac{p_{2,3;0}-p_{2,1;0}}{\frac{1}{2}h_{y_{3;0}}+h_{y_{2;0}}+\frac{1}{2}h_{y_{1;0}}}$. It is used to approximate the tangential line through $p_{2,2;0}$. Finally, the approximations for $p_{2,2;0-}$ and $p_{2,2;0+}$ are found at this line by making a step of size $|y_{p_{2,2;0+}} - y_{p_{2,2;0}}| = |y_{p_{2,2;0}} - y_{p_{2,2;0-}}| = h_{y_{5;1}}$ in the y-direction along this line. Generally, the approximation of the tangential line by this procedure is very poor, but it is in analogy to the construction of the skew-symmetric discretization, which has been proven to behave very well (see [7]).

Having constructed the gradient matrix G and successively the divergence matrix M by applying (2), we can continue our adaptation process by adapting the convective matrix C. There are two cases:

- the refinement boundary is along the boundary of a conservation cell;
- the refinement boundary crosses a conservation cell.

At the beginning of this section, we sketched the way to proceed in both cases. Now, we still need interpolations to make up for the missing velocities. As for the pressure, linear interpolation will not work. For then the mass fluxes can not be chosen such that the central convective coefficient becomes zero. So, we use more points and take (with respect to Figure 4)

$$u_{2,2;0-} = u_{2,2;0} - \frac{h_{y_{5;1}}(u_{2,3;0} - u_{2,1;0})}{\frac{1}{2}h_{y_{3;0}} + h_{y_{2;0}} + \frac{1}{2}h_{y_{1;0}}}, \quad (12)$$

$$u_{2,2;0+} = u_{2,2;0} + \frac{h_{y_{5;1}}(u_{2,3;0} - u_{2,1;0})}{\frac{1}{2}h_{y_{3;0}} + h_{y_{2;0}} + \frac{1}{2}h_{y_{1;0}}} \quad (13)$$

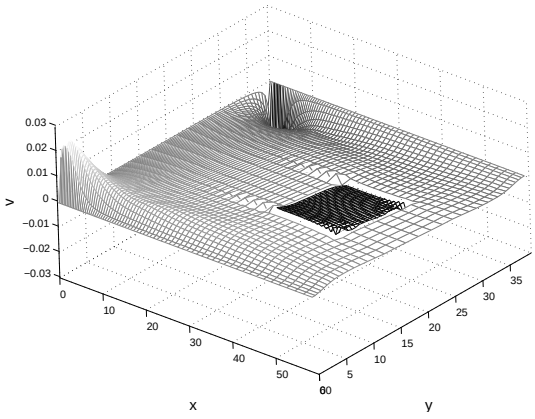

Figure 6: Global view of the v-velocity for $Re = 100$ at an intermediate fine grid. The region of local grid refinement is clearly visible.

and

$$v_{2,1;0+} = \frac{1}{2}(v_{2,1;0} + v_{2,2:0}) - \frac{\frac{1}{2}h_{y_{5;1}}(v_{2,3;0} - v_{2,0;0})}{h_{y_{3;0}} + h_{y_{2;0}} + h_{y_{1;0}}}, \quad (14)$$

$$v_{2,2;0-} = \frac{1}{2}(v_{2,1;0} + v_{2,2:0}) + \frac{\frac{1}{2}h_{y_{5;1}}(v_{2,3;0} - v_{2,0;0})}{h_{y_{3;0}} + h_{y_{2;0}} + h_{y_{1;0}}}. \quad (15)$$

For the extrapolations (12)-(15), it is possible to determine the coefficients of the convective matrix C in such a way that it becomes skew-symmetric.

With this, we have reached a complete discretization. However, we expect to see some problems at the refinement boundaries as in literature many investigators have observed reflections coming from refinement boundaries (e.g. [2] and [4]).

4 Tests

The behaviour of the derived discretizations has been tested for Poiseuille flow in a channel with length×height 60×39. The Reynolds number was based on the width of the channel and the uniform inflow velocity, creating main flow in the x-direction. The computational grid was similar to the one depicted in Figure 2, with the refinement between $x = 34$ and $x = 48$ and between $y = 14$ and $y = 25$ as one can see in Figures 6 and 7.

In the tests, the global results were all right. This means that the u-velocity becomes parabolic, the v-

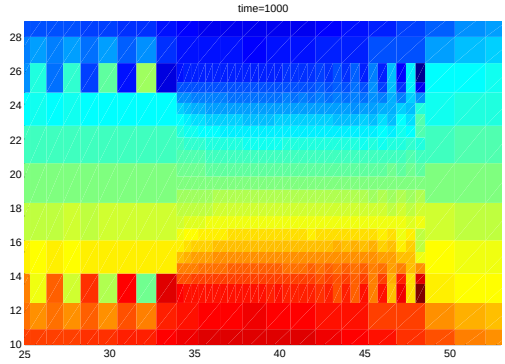

Figure 7: Detail of the v-velocity of Figure 6 in top view. It shows the region of local grid refinement and its direct surroundings. Wiggles (with a magnitude of about $1.2 \cdot 10^{-3}$) are clearly visible.

velocity tends to zero and the pressure becomes linearly decreasing with x. Figure 6 shows the v-velocity at $Re = 100$ for example. As predicted, observations of details revealed some wiggles in the solution heading backwards, see Figure 7. However, those wiggles were only originating at the corners of the refinement and not at the straight edges as one might expect from [4].

The development of these wiggles was studied for several mesh sizes and Reynolds numbers. The wiggles were measured in the v-velocity, because they were seen best there. Two positions of origination of the wiggles were used as measure points; one was in the coarse part just before the flow entered the refinement and one was in the fine part just before the flow left the refinement. At these positions, the strength of the wiggles was measured by taking the mean wiggles size over four cells. So, the wiggle strength was calculated as

$$\left| \frac{1}{8}(v_{i,j;m} - v_{i-1,j;m}) + \frac{1}{8}(-v_{i-1,j;m} + v_{i-2,j;m}) + \frac{1}{8}(v_{i-2,j;m} - v_{i-3,j;m}) + \frac{1}{8}(-v_{i-3,j;m} + v_{i-4,j;m}) \right|. \quad (16)$$

Figure 8 shows the results of these measurements. In this figure, we can observe $O(h^2)$ (and sometimes even $O(h^3)$) convergence behaviour for all Reynolds numbers except $Re = 1$. This exception is not remarkable as for $Re = 1$ there were no wiggles in the

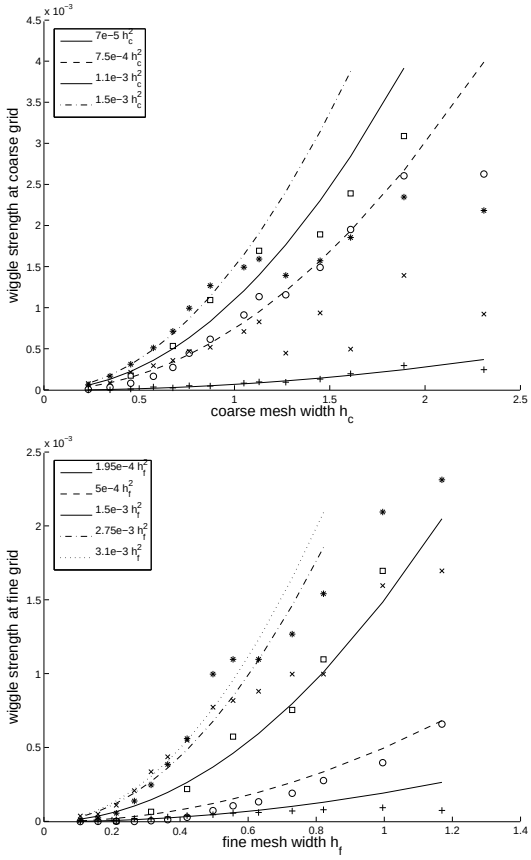

Figure 8: The wiggle strength versus the mesh size for several Reynolds numbers. Top: the wiggle strength at the coarse grid measure point. Bottom: the wiggle strength at the fine grid measure point. $+$: $Re = 1$; $\circ$: $Re = 10$; $\square$: $Re = 30$; $*$: $Re = 100$; $\times$: $Re = 1000$.

solution and merely the variation in the solution was measured. It may also be noted that the convergence behaviour becomes irregular for larger cell sizes because the Peclet number (based on the local velocity and mesh size and the Reynolds number) becomes too large, i.e. larger than 2 (estimations for $Re = 1$, 10, 30, 100 and 1000 are that the coarse mesh width must be smaller than 75, 7.5, 2.5, 0.75 and 0.075, respectively).

From Figure 8, we conclude that the wiggles depend on a numerical factor, the mesh width, as well as physical factors contained in the Reynolds number. So, the wiggle strength can be described as

$$\alpha(Re)h^2 + O(h^3). \quad (17)$$

The unknown values of the physical contribution function α are approximated by the coefficients of the parabolas drawn to interpolate the data for each Reynolds number. We get an impression of the physi-

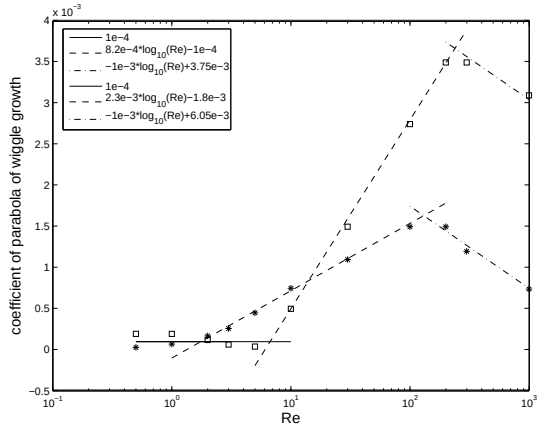

Figure 9: The coefficients of the parabolas interpolating the wiggle growth versus the Reynolds number. The □'s are related to the fine grid measurement, the $*$'s to the coarse grid measurement.

cal contribution function by plotting these coefficients against the Reynolds number. This is done in Figure 9. We can clearly see the region with no wiggles for low Reynolds numbers. For higher Reynolds numbers, the coefficients indicate that wiggles can grow. In the right region, we see the effect of the Peclet number in the simulations becoming too large: the coefficient of the interpolating parabola could not be determined properly. Also, we observe a factor 3 in the Reynolds number at which wiggles can start to grow at the coarse and fine mesh (2 versus 6) and a 3:1 ratio in the gradients of the lines in the middle region. These last two observation might be related to the 3:1 refinement ratio as well.

5 Conclusions

In this paper, we have constructed a skew-symmetric discretization of convection with local grid refinement. To do this, we have adapted the discrete gradient and divergence. The discretization of the diffusion in case of local grid refinement, which has not been discussed in this paper, can be made using the same velocities as the convective discretization, but this is not necessary.

The constructed discretizations have been tested for Poiseuille flow. They seem to perform well except at the corners of the refinement, where wiggles are originating at higher Reynolds numbers. These wiggles were shown to have at least $O(h^2)$ convergence behaviour. Also, the dependence of these wiggles on the Reynolds number has been investigated. It was found that the higher the Reynolds number was, the larger the wiggle amplitude became.

In the near future, we will try to apply this method in a simulation of the flow around a rectangular cylinder at $Re = 22000$ (see [6]). Then we will answer the questions whether we can be as accurate as without local grid refinement and how much reduction of computational effort we can achieve.

Acknowledgements:
This research was supported by the Netherlands Organisation for Scientific Research (NWO).

References:

[1] G. Agresar, J.J. Linderman, G Tryggvason and K.G. Powell, An Adaptive, Cartesian, Front-Tracking Method for the Motion, Deformation and Adhesion of Circulating Cells, *Journal of Computational Physics*, Vol. 143, 1998, pp. 346-380

[2] D. Choi, J.D. Brown, B. Imbiriba, J. Centrella and P. MacNeice, Interface Conditions for Wave Propagation through Mesh Refinement Boundaries, *Journal of Computational Physics*, Vol. 193, 2004, pp. 398-425

[3] M. Dröge, *Local Mesh Refinement*, Master's thesis, University of Groningen, 2000

[4] J. Frank and S. Reich, On Spurious Reflections, Nonuniform Grids and Finite Difference Discretizations of Wave Equations, available at *http://www.ma.ic.ac.uk/~sreich/publications.html*

[5] S.S. Ochs and R.G. Rajagopalan, An Adaptively Refined Quadtree Grid Method for Incompressible Flows, *Numerical Heat Transfer, Part B*, Vol. 34, 1998, pp. 379-400

[6] R.W.C.P. Verstappen and A.E.P. Veldman, Spectro-consistent Discretization of Navier-Stokes: a Challenge to RANS and LES, *Journal of Engineering Mathematics*, Vol. 34, No. 1-2, 1998, pp. 163-179

[7] R.W.C.P. Verstappen and A.E.P. Veldman, Symmetry-preserving Discretization of Turbulent Flow, *Journal of Computational Physics*, Vol. 187, 2003, pp. 343-368